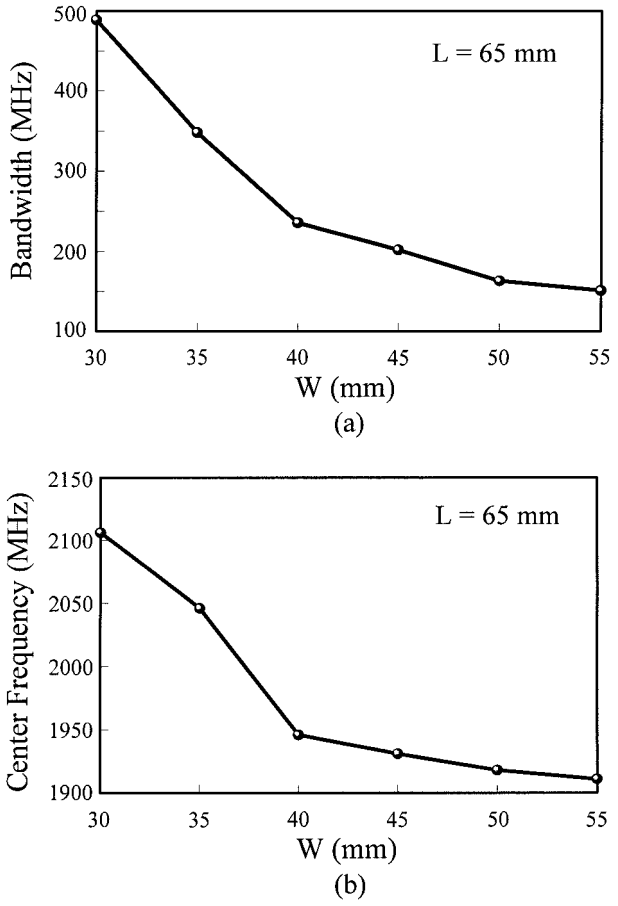

Figure 4 Measured (a) impedance bandwidth and (b) center operating frequency for the antenna shown in Figure 1 with $L = 65$ mm

ground-plane length (about 45% of the free-space wavelength at 2050 MHz) for achieving maximum impedance bandwidth. On the other hand, there is a critical value for the ground-plane width (about 27% of the free-space wavelength at 2050 MHz); when the ground-plane width is less than the critical value, relatively very sharp variations in the impedance bandwidth have been seen.

REFERENCES

1. S. Tarvas and A. Isohatala, An internal dual-band mobile phone antenna, 2000 IEEE Antennas Propagat Soc Int Symp Dig, Salt Lake City, UT, pp. 266–269.
2. Z.D. Liu, P.S. Hall, and D. Wake, Dual-frequency planar inverted-F antenna, IEEE Trans Antennas Propagat 45 (1997), 1451–1458.
3. C.R. Rowell and R.D. Murch, A capacitively loaded PIFA for compact mobile telephone handsets, IEEE Trans Antennas Propagat 45 (1997), 837–842.
4. W.P. Dou and Y.W.M. Chia, Novel meandered planar inverted-F antenna for triple-frequency operation, Microwave Opt Technol Lett 27 (2000), 58–60.
5. P. Salonen, M. Keskilammi, and M. Kivikoski, New slot configurations for dual-band planar inverted-F antenna, Microwave Opt Technol Lett 28 (2001), 293–298.
6. G.K.H. Lui and R.D. Murch, Compact dual-frequency PIFA designs using LC resonators, IEEE Trans Antennas Propagat 49 (2001), 1016–1019.
7. M. Martinez-Vazquez, M. Geissler, and D. Heberling, Volume considerations in the design of dual-band handset antennas, 2001 IEEE Antennas Propagat Soc Int Symp Dig, Boston, MA, pp. 112–115.
8. D. Manteuffel, A. Bahr, D. Heberling, and I. Wolff, Design considerations for integrated mobile phone antennas, Proc 2001 IEE Int Conf Antennas Propagat, Manchester, England, pp. 252–254.

TIME-DOMAIN FINITE-ELEMENT SIMULATION OF CAVITY-BACKED MICROSTRIP PATCH ANTENNAS

Dan Jiao[1] and Jian-Ming Jin[1]
[1] Center for Computational Electromagnetics
Department of Electrical and Computer Engineering
University of Illinois at Urbana–Champaign
Urbana, Illinois 61801-2991

Received 30 August 2001

ABSTRACT: *A time-domain finite-element method (TDFEM) is presented for simulating the radiation and scattering from cavity-backed microstrip patch antennas. The perfectly matched layer (PML) is utilized to efficiently truncate the TDFEM solution domain. The higher order vector basis functions are adopted to accurately represent unknown fields. Numerical examples are given to demonstrate its efficacy.* © 2002 John Wiley & Sons, Inc. Microwave Opt Technol Lett 32: 251–254, 2002.

Key words: *finite-element method; microstrip patch antennas; scattering time domain*
DOI 10.1002 / mop.10146

1. INTRODUCTION

Cavity-backed microstrip patch antennas are highly resonant structures. Their characteristics, such as the input impedance, vary drastically as a function of frequency. This increases the modeling difficulty when conventional frequency-domain-based methods are used for simulation since a set of algebraic equations must be solved repeatedly at many isolated frequency points. In this paper, a time-domain finite-element method (TDFEM) is presented to analyze the radiation and scattering from cavity-backed microstrip patch antennas. This method utilizes the perfectly matched layers (PMLs) to truncate the TDFEM solution domain, and the implementation is based on a recently developed algorithm in [1, 2]. The time-domain simulation captures the drastically varying frequency responses with one calculation. The finite-element analysis enhances the geometry-modeling capability. The adoption of higher order vector basis functions accurately describes the unknown fields. The utilization of PMLs permits the absorption of outgoing waves with any polarizations and at any frequencies and angles of incidence. Numerical results are compared with those obtained by measurements and the frequency-domain finite-element–boundary-integral (FDFE–BI) method.

2. FORMULATION

Consider a cavity-backed microstrip patch antenna recessed in a ground plane (Fig. 1). To formulate the TDFEM solution, we introduce a PML over the aperture S_a to entirely enclose the computational domain V_o. Inside V_o, the electric

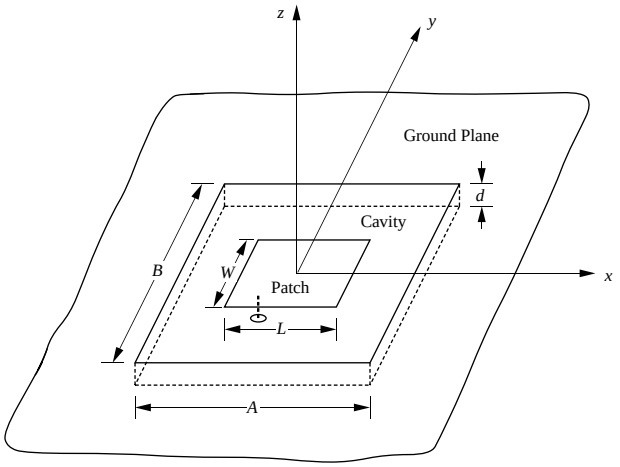

Figure 1 Geometry of a cavity-backed microstrip patch antenna

field satisfies the second-order vector wave equation

$$\nabla \times \mu^{-1}\overline{\Lambda}^{-1}(\mathbf{r},t) * \nabla \times \tilde{\mathbf{E}}(\mathbf{r},t) + \sigma\partial_t\tilde{\mathbf{E}}(\mathbf{r},t) + \epsilon\overline{\Lambda}(\mathbf{r},t) * \partial_t^2\tilde{\mathbf{E}}(\mathbf{r},t) = -\partial_t\mathbf{J}^{\text{int}}(\mathbf{r},t) - \mu^{-1}\nabla \times \mathbf{M}^{\text{int}}(\mathbf{r},t) \quad (1)$$

where $\mathbf{J}^{\text{int}}(\mathbf{r},t)$ and $\mathbf{M}^{\text{int}}(\mathbf{r},t)$ denote the electric and magnetic sources associated with the antenna feeds, $*$ stands for temporal convolution, conductivity σ is introduced to characterize the loss of the substrate and the impedance load, $\tilde{\mathbf{E}}(\mathbf{r},t)$ denotes the stretched electric field, and $\overline{\Lambda}(\mathbf{r},t)$ is the time-domain counterpart of the diagonal tensor [3]:

$$\overline{\Lambda} = \hat{x}\hat{x}\left(\frac{S_yS_z}{S_x}\right) + \hat{y}\hat{y}\left(\frac{S_xS_z}{S_y}\right) + \hat{z}\hat{z}\left(\frac{S_xS_y}{S_z}\right) \quad (2)$$

where $S_\xi(\xi = x, y, z)$ are the stretching variables given by

$$S_\xi = 1 + \frac{\sigma_\xi}{j\omega\epsilon_0}, \qquad \xi = x, y, z. \quad (3)$$

Based on the algorithm developed in [2], the TDFEM solution of (1) results in an ordinary differential equation:

$$\mathbf{T}\frac{d^2u}{dt^2} + (\mathbf{T}_p + \mathbf{R})\frac{du}{dt} + \mathbf{Q}\frac{du}{dt} + \mathbf{T}_q u + \mathbf{S}u + \sum_{\xi=x,y,z}\mathbf{S}_\xi\psi_\xi + \sum_{\xi=x,y,z}\mathbf{T}_\xi\psi_\xi = -f^{\text{int}} \quad (4)$$

where $\mathbf{T}$, $\mathbf{T}_p$, $\mathbf{R}$, $\mathbf{Q}$, $\mathbf{T}_q$, $\mathbf{S}$, $\mathbf{S}_\xi$, and $\mathbf{T}_\xi(\xi = x, y, z)$ are square matrices, and f^{int} denotes the excitation vector

$$f^{\text{int}} = \langle \mathbf{N}_i, \partial_t\mathbf{J}^{\text{int}}\rangle_{V_o} + \langle \mu^{-1}\nabla \times \mathbf{N}_i, \mathbf{M}^{\text{int}}\rangle_{V_o} \quad (5)$$

where $\mathbf{N}_i$ denotes the vector basis function.

For scattering analysis, the solution is formulated in terms of the scattered field, and for radiation analysis, it uses the total radiated field. For the spatial discretization, the unknown fields are expanded using higher order edge elements [4]. For the temporal discretization, the Newmark method is employed for time marching.

One of the important issues in the antenna simulation is the modeling of feeds and loads. The coaxial feed is commonly used as antenna excitation. For thin substrates, a coaxial feed can be replaced by a current filament $I(t)$. The excitation vector in (5) becomes

$$f^{\text{int}} = \partial_t I(t) l \iint \hat{z} \cdot \mathbf{N}_i \delta(x - x_f)\delta(y - y_f)\,dx\,dy \quad (6)$$

where l is the length of the current filament, and (x_f, y_f) denotes the position of the current source. Clearly, f^{int} is a vector whose elements are zero, except for the ith element, which is equal to $\partial_t I(t) l$ if the basis function $\mathbf{N}_i$ is normalized. If higher order vector bases are used to expand the unknown fields, the current filament can be partitioned into several segments to consider its contribution since one edge is associated with more than one degree of freedom. For thicker substrates, a magnetic frill current $\mathbf{M}^{\text{int}}(\mathbf{r},t)$ can be introduced over the aperture of the coaxial feed, while the inner conductor of the feed is modeled as a conducting post [5].

An impedance load of Z_L in Ω can be modeled as a post of finite conductivity connecting the patch to the base of the cavity. Its contribution to matrix $\mathbf{R}$ in (4) can be written as

$$\mathbf{R}_{ij} = d^2 Z_L^{-1} \iint \mathbf{N}_i \cdot \mathbf{N}_j \delta(x - x_L)\delta(y - y_L)\,dx\,dy \quad (7)$$

where d is the length of the post, and (x_L, y_L) denotes the position of the impedance load. If the post coincides with the ith edge, it only contributes to the ith diagonal element of matrix $\mathbf{R}$, which amounts to adding $d^2Z_L^{-1}$ to $\mathbf{R}_{ii}$. If higher order basis functions are used, similar to the case of antenna feeds, the conducting post can be partitioned into several segments to consider its contribution. If the shorting pins are used, one can simply set the tangential electric field along the post to zero or specify a large conductivity for the conducting post.

The TDFEM scheme calculates near fields. The far-field signature, such as the radar cross section (RCS), can be computed as

$$\text{RCS} = \lim_{r\to\infty} 4\pi r^2 \frac{|\mathcal{F}\{\mathbf{H}^{\text{far}}(\mathbf{r},t)\}|^2}{|\mathcal{F}\{\mathbf{H}^{\text{inc}}(\mathbf{r},t)\}|^2} \quad (8)$$

where the far-zone scattered magnetic field $\mathbf{H}^{\text{far}}$ can be calculated from

$$\mathbf{H}^{\text{far}}(t + c^{-1}r) = (2\pi rc\eta_0)^{-1}\partial_t\left(\hat{\theta}\hat{\theta} + \hat{\phi}\hat{\phi}\right)\mathbf{L}(\mathbf{r},t) \quad (9)$$

in which $\mathbf{L}(\mathbf{r},t)$ relates to the integration of the equivalent magnetic current $\mathbf{K}$ over the aperture S_a:

$$\mathbf{L}(\mathbf{r},t) = \iint_{S_a} \mathbf{K}(x', y', t + c^{-1}\hat{\mathbf{r}} \cdot \mathbf{r}')\,dx'\,dy'. \quad (10)$$

3. NUMERICAL EXAMPLES

The first example is scattering by an antenna consisting of a 3.66 cm × 2.60 cm rectangular conducting patch residing on a dielectric substrate having thickness $t = 0.158$ cm, relative permittivity $\epsilon_r = 2.17$, and conductivity $\sigma = 0.604$ ms/m. The substrate is housed in a 7.32 cm × 5.20 cm rectangular cavity recessed in a ground plane. The PML wraps the aperture,

and is 1 cm thick. The vertical distance from the PML to the aperture is 1 cm. The PML is formulated in a quadratic profile, and the maximum conductivity is chosen to be 0.9 s/m. The computational domain is discretized into 10,455 tetrahedra, yielding 66,338 unknowns with the use of the first-order vector basis functions. The incident pulse is specified as

$$\mathbf{E}^{\text{inc}}(\mathbf{r},t) = \hat{\theta}2[t - t_0 - c^{-1}\hat{\mathbf{k}}\cdot(\mathbf{r}-\mathbf{r}_0)] \times \exp\left\{-[t - t_0 - c^{-1}\hat{\mathbf{k}}\cdot(\mathbf{r}-\mathbf{r}_0)]^2/\tau^2\right\}$$

in which $t_0 = 0.49$ ns, $\tau = 0.098$ ns, $\mathbf{r}_0 = \hat{z}2$ cm, and $\hat{\mathbf{k}} = -\hat{x}\sin 60^\circ\cos 45^\circ - \hat{y}\sin 60^\circ \sin 45^\circ - \hat{z}\cos 60^\circ$. Figure 2 shows the temporal backscattered far-field signatures. The monostatic RCS of the antenna is shown in Figure 3 as a function of frequency from 2 to 8 GHz. Clearly, the RCS is characterized by a series of peaks, each corresponding to a resonant mode of the patch. The result compares well with that generated by FDFE–BI, and the experimental data for the patch residing on an infinite substrate [6].

The second example is radiation by an antenna consisting of a 5.0 cm × 3.4 cm rectangular conducting patch residing

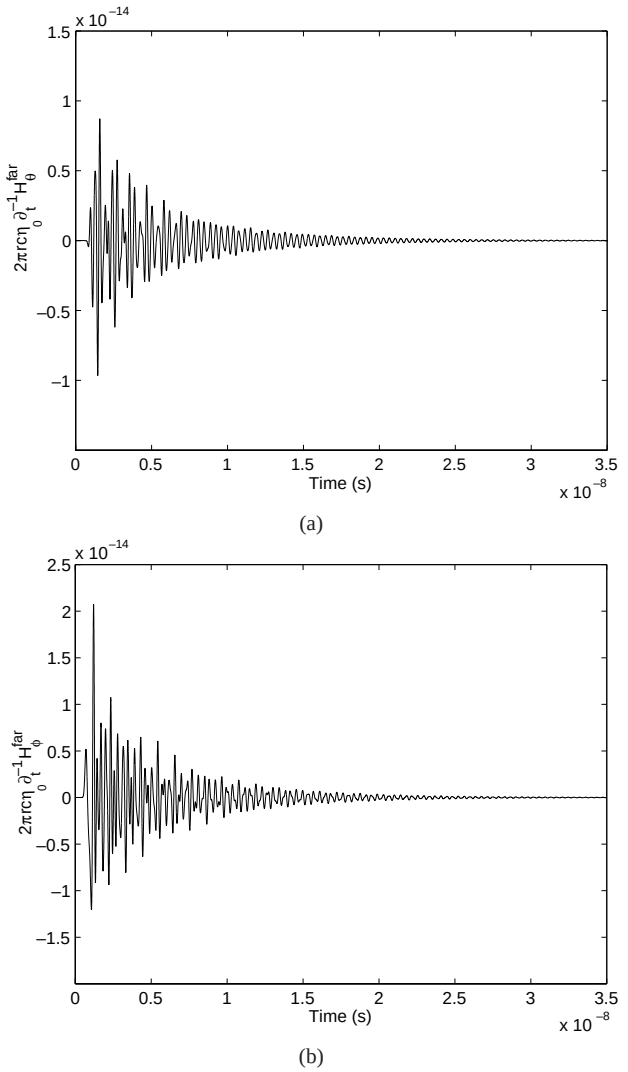

Figure 2 Backscattered far-field temporal signatures. (a) $2\pi rc\eta_0\partial_t^{-1}\mathbf{H}_\theta^{\text{far}}$. (b) $2\pi rc\eta_0\partial_t^{-1}\mathbf{H}_\phi^{\text{far}}$

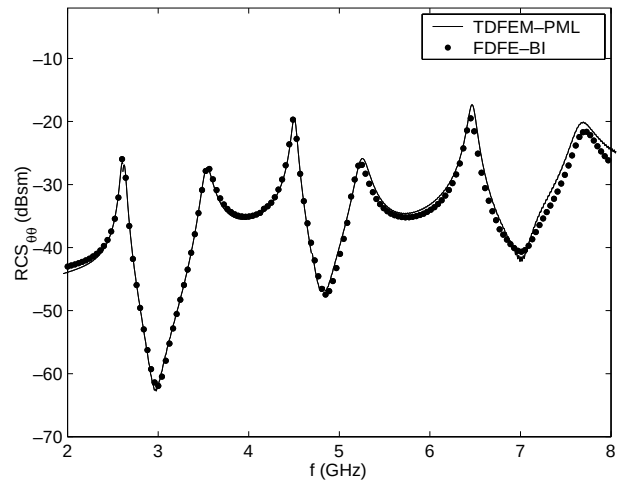

Figure 3 Monostatic VV-polarized RCS versus frequency for a cavity-backed patch antenna ($A = 7.32$ cm, $B = 5.20$ cm, $L = 3.66$ cm, $W = 2.60$ cm, $d = 0.158$ cm, $\epsilon_r = 2.17$, $\tan\delta = 0.001$, $\theta^{\text{inc}} = 60^\circ$, $\phi^{\text{inc}} = 45^\circ$)

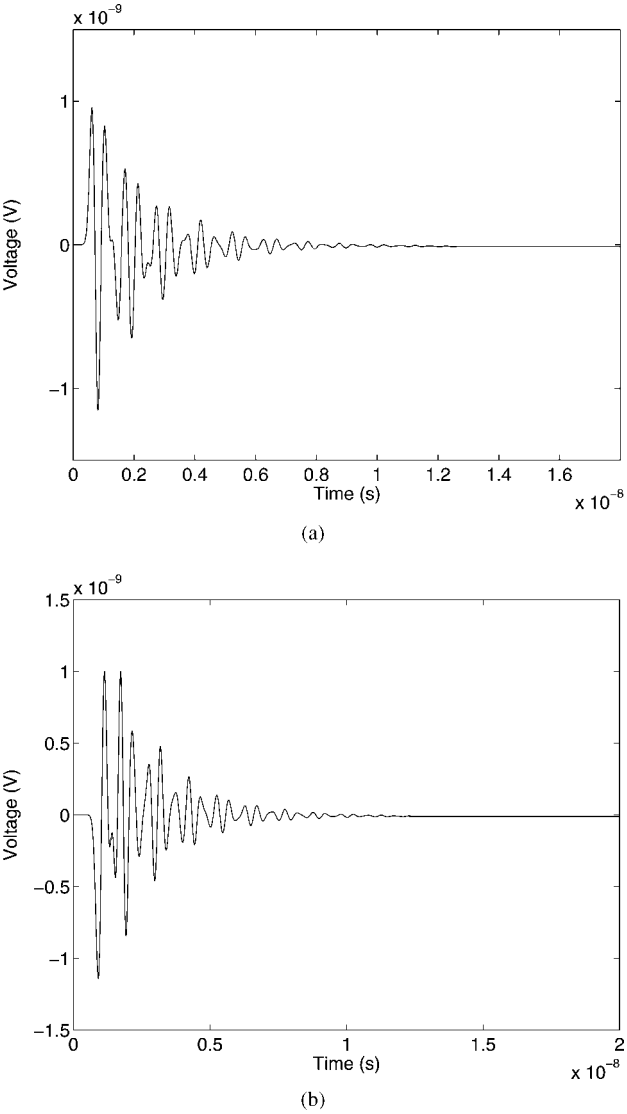

Figure 4 Sampled voltage waveforms at (a) the input port and (b) the impedance load

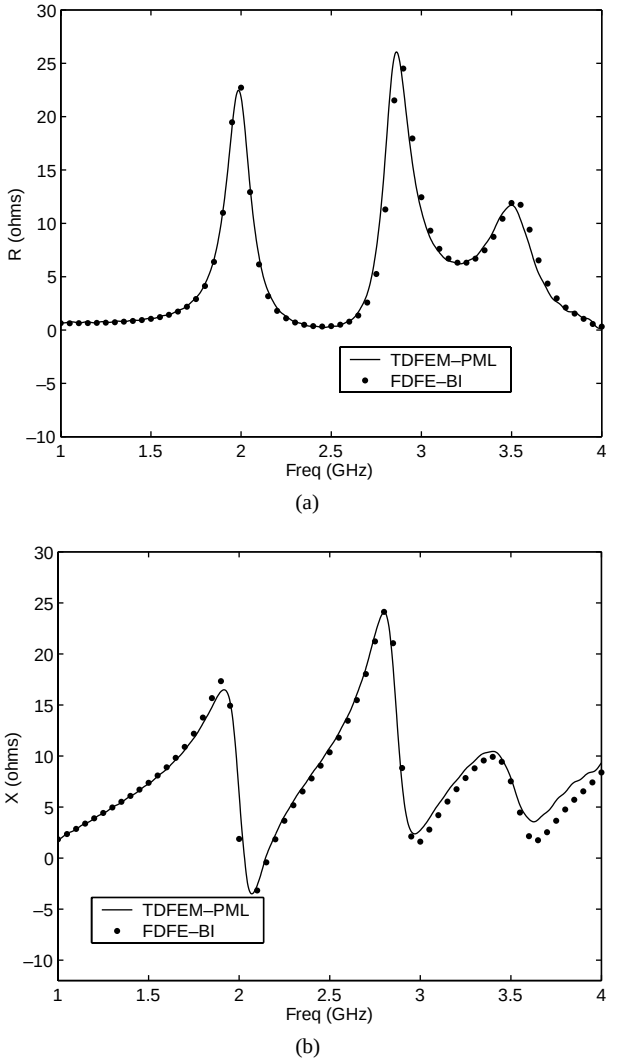

Figure 5 Input impedance versus frequency for a cavity-backed patch antenna with a probe feed at $x_f = 1.22$ cm and $y_f = 0.85$ cm, and a 50 Ω impedance load at $x_L = -2.2$ cm and $y_L = -1.5$ cm ($A = 7.5$ cm, $B = 5.1$ cm, $L = 5.0$ cm, $W = 3.4$ cm, $d = 0.08779$ cm, $\epsilon_r = 2.17$, $\tan\delta = 0.0015$). (a) Resistance. (b) Reactance

on a dielectric substrate having thickness $t = 0.08770$ cm, relative permittivity $\epsilon_r = 2.17$, and conductivity $\sigma = 0.362$ ms/m. The substrate is housed in a 7.5 cm × 5.1 cm rectangular cavity recessed in a ground plane. The PML has a thickness of 1 cm, and is placed in the same fashion as in the previous example, except that the vertical distance is reduced to 0.1 cm. The entire computational region is subdivided into 6419 tetrahedra, generating 40,438 unknowns with the use of the first-order vector basis functions. The patch is excited by a current probe applied at $x_f = 1.22$ cm and $y_f = 0.85$ cm, with a current pulse

$$I_z(t) = 2(t - t_0)\exp\left[-(t - t_0)^2/\tau^2\right] \qquad (11)$$

where $t_0 = 0.78$ ns and $\tau = 0.16$ ns. A 50 Ω impedance load is placed at $x_L = -2.2$ cm and $y_L = -1.5$ cm. Figure 4 shows the calculated voltage at the input port and the impedance load, respectively. Figure 5 shows the input impedance of the antenna as a function of frequency from 1 to 4 GHz. The calculated results compare well with that obtained by FDFE–BI, and the experimental data for the patch residing on an infinite substrate [6].

4. CONCLUSION

A TDFEM scheme is presented for the analysis of cavity-backed microstrip patch antennas. The method uses the PML for truncating the finite-element solution domain and the higher order vector basis functions for expanding the electric field. Numerical examples are given to demonstrate its validity.

REFERENCES

1. D. Jiao and J.M. Jin, An effective algorithm for implementing perfectly matched layers in time-domain finite-element simulation of open-region EM problems, University of Illinois, tech rep CCEM9-01, 2001.
2. D. Jiao, J.M. Jin, E. Michielssen, and D. Riley, Time-domain finite-element simulation of three-dimensional scattering and radiation problems using perfectly matched layers, University of Illinois, tech rep CCEM11-01, 2001.
3. S.D. Gedney, An anisotropic perfectly matched layer-absorbing medium for the truncation of FDTD lattices, IEEE Trans Antennas Propagat 44 (1996), 1630–1639.
4. R.D. Graglia, D.R. Wilton, and A.F. Peterson, Higher order interpolatory vector bases for computational electromagnetics, IEEE Trans Antennas Propagat 45 (1997), 329–341.
5. J.M. Jin, The finite element method in electromagnetics, Wiley, New York, 1993.
6. D.P. Forrai and E.H. Newman, Radiation and scattering from loaded microstrip antennas over a wide bandwidth, Ohio State University, tech rep 719493-1, 1988.

BROADBAND HYBRID MICROSTRIP COUPLERS — AMPLITUDE AND PHASE

Cham Kiong Queck[1] and Lionel E. Davis[1]
[1] Microwave Engineering Group
Department of Electrical Engineering and Electronics
University of Manchester Institute of Science and Technology
Manchester M60 1QD, England

Received 3 September 2001

ABSTRACT: *Several designs for a 180° hybrid coupler are discussed. Using the stepped-impedance method, the bandwidth of an 11 GHz hybrid coupler is increased to approximately 1.6 times the bandwidth of a conventional hybrid coupler. Comparisons are made between conventional and broadband hybrid couplers, as well as between circular and rectangular designs, and the phase behavior of each is compared for the first time.* © 2002 John Wiley & Sons, Inc. Microwave Opt Technol Lett 32: 254–259, 2002.

Key words: *hybrid coupler; broadband; microstrip; phase*
DOI 10.1002 / mop.10147

1. CONVENTIONAL 180° HYBRID COUPLER

180° hybrid couplers are commonly used in the design of microwave and millimeter-wave devices such as balanced mixers, modulators, frequency multipliers, and amplifiers. There is also an application in which a hybrid coupler can be integrated with a ferrite coupled-line (FCL) structure to produce a novel four-port FCL circulator. The performance of these circulators may be limited by the bandwidth of the